

**Nonequilibrium electron dynamics in materials driven by high-intensity x-ray pulses**

Stefan P. Hau-Riege\*

*Lawrence Livermore National Laboratory, Livermore, California 94550, USA*

(Received 24 January 2013; published 7 May 2013)

We calculated the evolution of the electron system in solid-density matter irradiated by high-intensity x-ray pulses between 2 and 8 keV using molecular dynamics. For pulses shorter than 40 fs, the kinetic energy distribution of the electrons is highly nonthermal during and right after the pulse, and a large fraction of the absorbed x-ray energy resides with the fast photoelectrons which equilibrate on the timescale of the pulse length. The average ionization and electron temperature of the bulk of the electrons are significantly lower than their equilibrium values.

DOI: [10.1103/PhysRevE.87.053102](https://doi.org/10.1103/PhysRevE.87.053102)

PACS number(s): 52.25.Os, 61.80.Az

**I. INTRODUCTION**

High-intensity and short-duration x-ray pulses emitted by x-ray free-electron lasers (XFELs) offer unprecedented opportunities for studying fundamental dense plasma physics phenomena. XFEL pulse lengths of tens of fs or shorter are so brief that hydrodynamic expansion and associated inhomogeneities during the exposure can usually be neglected. In contrast to optical laser experiments, x rays penetrate solid-density materials, and the total amount of absorbed energy is known since the predominant inner-shell x-ray absorption process depends only weakly on the plasma environment. Recent applications include the characterization of atomic states in dense plasmas through fluorescence [1], measurements of electron-ion equilibration time scales [2,3], and studies of nanoplasma dynamics [4–6].

The first hard XFEL, the Linac Coherent Light Source (LCLS), was designed to emit 230-fs-long x-ray pulses [7], but, actually, pulse durations ranging from only 10 fs to typically 40 fs [7] have been achieved. For such short times, the excited electron system is far from equilibrium during and right after the pulse. Instead of a Maxwellian distribution, the system consists of fast photo and Auger electrons in a sea of slow secondary electrons, which interact through free-free and bound-free scattering [2,8,9]. These nonequilibrium electron distributions cannot be adequately described by a single temperature, which has important implications for the behavior and description of XFEL-generated plasmas. For example, since the impact ionization cross section is roughly proportional to  $\log(E/\chi)/E$ , where  $\chi$  is the weighted-mean ionization potential [10], the fast electrons interact with the samples less effectively than slow electrons. Therefore, using a “temperature” related in some way to the average electron kinetic energy provides only an imprecise description of the ionization dynamics. More generally, many descriptions of important plasma physics phenomena such as continuum lowering and electron-ion equilibration rely on the electrons being in thermodynamic equilibrium among themselves [11,12], which is usually not the case in XFEL-irradiated materials.

In this paper we characterize the electron equilibration dynamics in low- $Z$  materials exposed to high-intensity x-ray radiation assuming realistic XFEL parameters. We use

molecular-dynamics simulations to quantify the deviation from the equilibrium distribution and its effect on the average ionization to characterize the temperature of the slow electrons and the average kinetic energy of the fast electrons and to determine the equilibration time scales. After describing our simulation technique, we will first discuss the electron-electron equilibration dynamics during the x-ray pulse and then the processes after the pulse has concluded. Finally, we will conclude this paper.

**II. MATERIALS AND METHODS**

Using the nonequilibrium classical molecular-dynamics plasma simulation code ddcMD [13], we simulated the evolution of solid, initially neutral carbon with a density of  $1 \text{ g/cm}^3$  exposed to 2-mJ x-ray radiation with an x-ray energy  $E$  ranging from 2 to 8 keV, a duration  $T$  between 10 and 40 fs, and a full-width-half-maximum focal size of 100 nm to  $1 \mu\text{m}$ . These conditions mimic the performance of current XFELs [7] and are typical for various applications, including the XFEL flagship experiment of biological imaging and structure determination (e.g., Ref. [14]). We assumed that the x-ray flux is constant in time for the duration of the pulse. We verified in a select number of cases that a possible time structure of the pulse as often observed in XFEL radiation [7] does not affect the results significantly. We also assumed that the x-ray pulse is uniform in space since space-charge effects confine the fast electrons to a small volume during the pulse [15]. ddcMD utilizes a velocity Verlet integration with a particle-centric domain decomposition method. Long-range Coulomb forces were calculated by the particle-particle-particle-mesh (P<sup>3</sup>M) method. Using temperature-dependent semiclassical potentials, the short-range part of the Coulomb interaction is softened within a distance set by the de Broglie wavelength [16] to avoid the classical Coulomb collapse of the plasma. Earlier simulation studies on hydrogen plasmas suggest that our results are insensitive to the specific choice of the form of the potential [17]. We incorporated quantum-atomistic processes using the “small ball” approach, which takes advantage of the short-range nature of screened-particle interactions in a dense plasma: Only quantum processes within a small region about a given ion are considered under careful consideration of the effects of the plasma environment on the two-particle interaction rates within that region [18]. For most simulations the system size was  $10^5$  particles.

\*hauriege1@llnl.gov

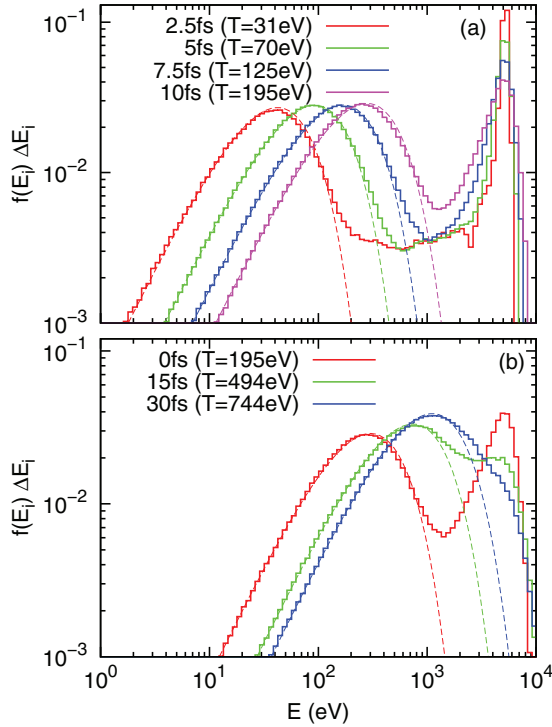


FIG. 1. (Color) (a) Evolution of the normalized electron velocity distribution of carbon irradiated with a 6-keV x-ray pulse, focused to 100 nm, for 10-fs (solid-step curve) and Maxwell distributions fitted to the low-energy part of the velocity distributions (dashed). (b) Relaxation of the bimodal electron velocity distribution after the x-ray pulse has been turned off.  $T$  is the temperature of the slow electrons.

For larger x-ray energies and smaller x-ray fluences, the effect of the x-ray beam on the material is weaker, and we increased the system size to up to  $10^7$  particles to improve the signal-to-noise ratio. We simulated infinitely large systems by assuming periodic boundary conditions. Finite-size effects such as sample charging and electron trajectories outside the sample are discussed in Ref. [15].

Figure 1(a) shows snapshots of the electron velocity distribution function  $f(E)$  of a carbon sample irradiated by a 6-keV x-ray pulse for 10 fs. The distributions exhibit two peaks: one low-energy feature made up of the secondary and a few Auger electrons and a high-energy peak from the photoelectrons. With time, the fast electrons heat the slow electrons and increase their number through elastic and inelastic scattering, respectively. Simultaneously, the fast electrons equilibrate among themselves, and the fast-electron peak broadens. For slower photoelectrons, for example, at 2 keV shown in Fig. 2(a), the slow and fast electron peaks eventually merge during the pulse. For smaller fluences, less energy is transferred to the slow electrons, and the peaks stay distinguishable; see Fig. 2(b).

To quantify the deviation of the bimodal velocity distribution  $f$  from equilibrium, we fit a Maxwellian kinetic energy distribution  $f_{\text{slow}}$  of temperature  $T_e$  to the low-energy peak, shown as dashed lines in Figs. 1 and 2. The remaining tail and high-energy peak of the distribution near the photon energy,  $f_{\text{fast}} = f - f_{\text{slow}}$ , are considered the fast electrons. We then define the fraction of the kinetic energy of the fast

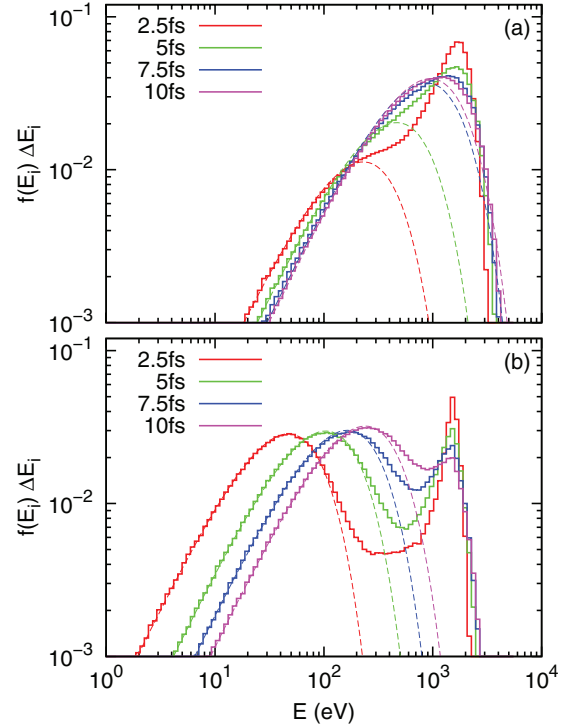


FIG. 2. (Color) (a) Evolution of the normalized electron velocity distribution of carbon irradiated with a 2-keV x-ray pulse, focused to 100 nm, for 10-fs (solid-step) and Maxwell distributions fitted to the low-energy part of the velocity distributions (dashed). (b) Similar results for a 10-times-larger focal diameter.

electrons relative to the total kinetic energy as  $\epsilon = E_{\text{fast}}/E_{\text{tot}} = \sum_i E_i f_{\text{fast}}(E_i) \Delta E_i / \sum_j E_j f(E_j) \Delta E_j$ . We chose  $\epsilon$  to measure the deviation from equilibrium since for many XFEL experiments, and the material behavior is determined by the temperature of the strongly interacting slow electrons, whereas the kinetic energy tied up by a few fast electrons is not affecting the material state significantly.

Figure 3 shows  $\epsilon$  as a function of normalized time  $t/T$  during the pulse for different pulse parameters. Early in the pulse,  $\epsilon = 1$  since mainly photoelectrons and only a few slow secondary electrons are present.  $\epsilon$  then decreases in time, primarily due to two processes: (i) inelastic scattering of the fast electrons associated with electron impact ionization until the material becomes mostly ionized and (ii) elastic electron-electron scattering once a sufficiently large number of slow electrons has been generated.  $\epsilon$  is generally smaller for 40-fs than for 10-fs pulses since longer pulses provide more opportunities for the system to equilibrate. For 10-fs pulses, most of the absorbed x-ray energy resides with the fast electrons [see Fig. 3(a)], except at 2 keV and 100-nm focal size, for which the slow electrons become so energetic that their distribution overlaps with the fast electrons [see Fig. 2(a)]. Further,  $\epsilon$  tends to be larger for larger x-ray energies since the slow- and fast-electron peaks are spectrally further apart; additionally, the interaction is weaker. Finally, for larger x-ray energies and larger beam diameters,  $\epsilon$  levels off for longer pulses. In this regime,  $T_e$ , the average ionization  $Z$ , and  $E_{\text{tot}}$  increase linearly in time, whereas the fraction of fast electrons and  $E_{\text{fast}}$  show only a slow increase.

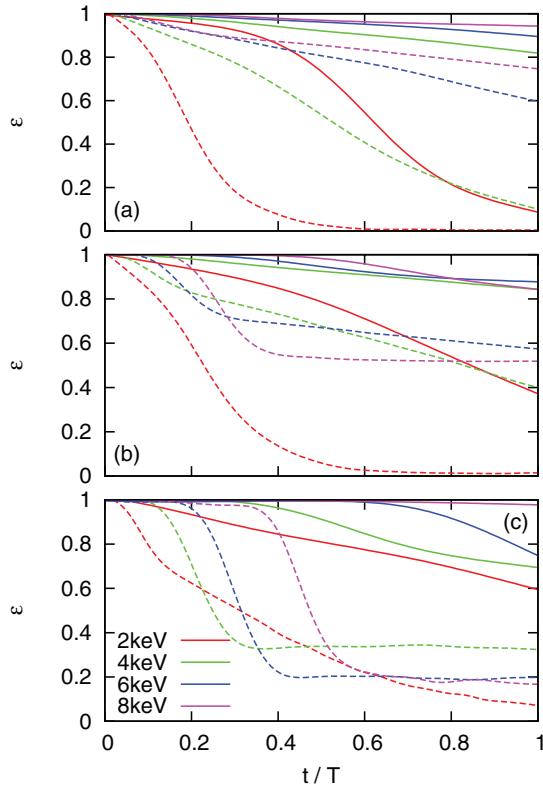


FIG. 3. (Color) Fraction  $\epsilon$  for focal sizes of (a) 100 nm, (b) 300 nm, and (c) 1  $\mu\text{m}$ . The pulse lengths are  $T = 10$  fs (solid) and  $T = 40$  fs (dashed).

The x-ray fluences considered in this paper are sufficient to create strongly ionized plasmas, but most of the ions stay in their atomic ground state during the pulse. Figure 4 shows  $Z$  and  $\epsilon$  at the end of the pulse. The ionization is larger for softer x rays and smaller focal diameters due to larger photoabsorption cross sections and larger x-ray fluences, respectively. For 100- and 300-nm focal sizes, the atomic L shell is (nearly) completely stripped for all x-ray energies. In the case of a 1- $\mu\text{m}$  focal size, the energy transfer is too slow during the 10-fs pulse to cause significant ionization for harder x rays; for the longer 40-fs pulses,  $Z \approx 3$  since the fast electrons had more time to transfer their kinetic energy.

Figure 4 shows also  $\epsilon$  at the end of the pulse. For 10-fs pulses,  $0.6 < \epsilon < 1$ , except for x-ray energies around 2 keV for which the slow electrons are so energetic that they are indistinguishable from the fast electrons. For 40-fs pulses, the system had more time to equilibrate, and  $0 < \epsilon < 0.5$ .  $\epsilon$  is smaller for softer x rays since the average kinetic energies of the slow and fast electrons are more similar.  $\epsilon$  increases with x-ray energy since the peaks are further apart and, finally, decreases again since bound-electron stopping eventually becomes effective ( $Z$  is small in this case).

The electrons continue to equilibrate after the end of the x-ray pulse; see Fig. 1(b) showing the electron distribution and Fig. 5 showing  $\epsilon$ . We define the equilibration time  $\tau$  as the time when 80% of the absorbed x-ray energy has been transferred to the slow electrons [ $\epsilon(\tau) = 20\%$ ]. Figure 6 shows  $\tau$  as a function of pulse parameters. For mostly ionized systems,  $\tau$  is larger for larger x-ray energies  $E$  since energetic

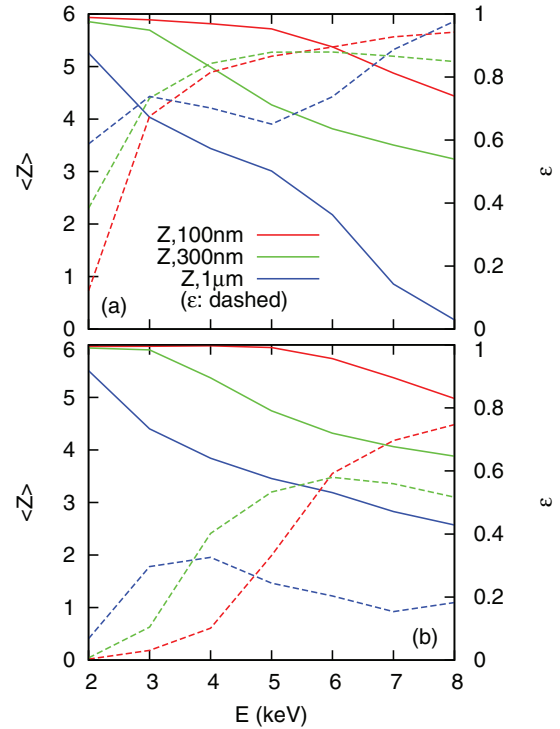


FIG. 4. (Color) Average ionization  $Z$  and  $\epsilon$  at end of pulse for (a) 10-fs and (b) 40-fs pulse lengths.

electrons interact more weakly than slower ones, and  $\epsilon$  is larger to begin with. For lower fluences, the ionization  $Z$  is smaller, and inelastic bound-free scattering leads to increased electron stopping at larger  $E$ . Further,  $\tau$  tends to be smaller for longer x-ray pulses since the system has already equilibrated somewhat during the pulse. In nearly all cases,  $\tau(E)$  roughly follows  $\epsilon(E)$  taken at end of pulse (Fig. 4), because it takes longer to reach  $\epsilon = 20\%$  when starting out from a larger value. We found that the  $\tau(E)$  as well as  $\epsilon(E)$  at  $t = T$  for 100- and 300-nm focal sizes intersect at  $E = 6$  keV because for 300 nm and  $E \geq 6$  keV, the L shell in carbon is populated, and bound stopping becomes more effective, whereas for smaller  $E$ , both  $\epsilon$  and  $\tau$  are smaller since the slow- and fast-electron peaks are closer. Finally, for the 1- $\mu\text{m}$  focal size, we again observe a

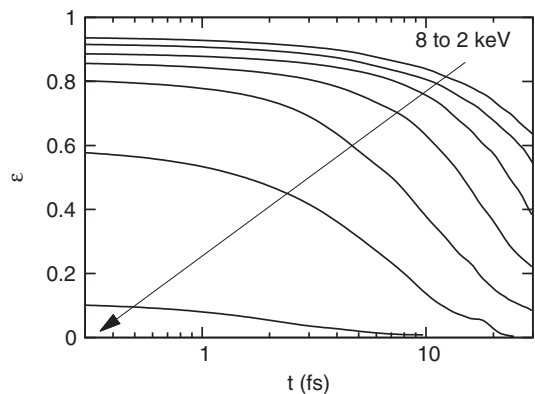


FIG. 5. Evolution of  $\epsilon$  after the 100-nm x-ray pulse with a duration of 10 fs.

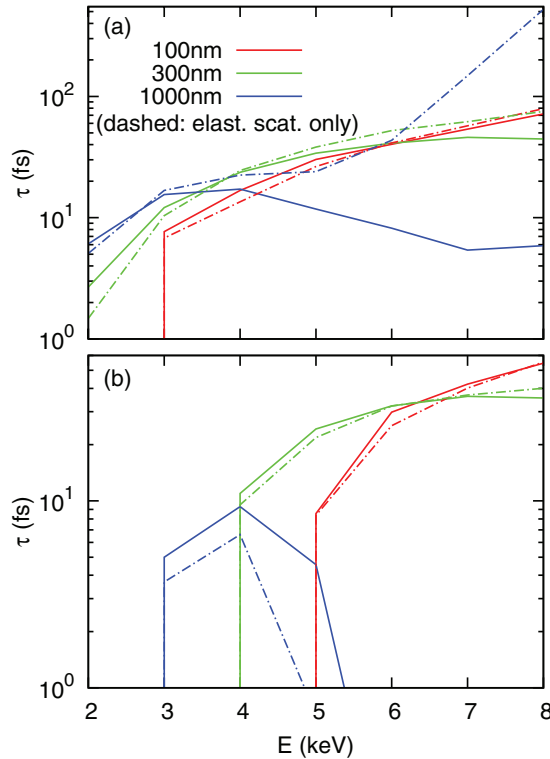


FIG. 6. (Color)  $\tau$  as a function of x-ray energy at the end of a (a) 10-fs- and (b) 40-fs-long x-ray pulse for different beam diameters (a) with atomic physics and (b) without atomic physics.

peak around 3 to 5 keV, and, for the same reasons, we observed a peak in  $\epsilon(T)$  [see Fig. 4(b)].

To determine the contribution of the bound electrons to fast-electron stopping, we calculated the evolution of  $\epsilon$  with the atomic physics processes turned off at the end of the x-ray pulse. We found that the bound electrons have little effect on the stopping in most cases since the systems are highly ionized, and K-shell electron-impact ionization is significantly weaker than for L-shell electrons. The most notable exceptions are 5- to 8-keV x-ray pulses that are 10 fs in duration and focused to 1  $\mu\text{m}$ , for which the L shell is somewhat populated [see Fig. 6(a)].

### III. CONCLUSIONS

In summary, we characterized the nonequilibrium electron distribution in strongly XFEL-driven dense plasmas and found that for pulse lengths of 40 fs and shorter, the distribution cannot be described by a single temperature since it is bimodal. The two peaks are more distinct for larger x-ray energies and shorter pulses. The slow-electron peak roughly follows a Maxwellian. The non-Maxwellian fast-electrons tie up a significant fraction of the absorbed x-ray energy.

The nonequilibrium nature of the electron distribution has important consequences for plasma experiments at XFELs: (i) The average ionization  $Z$  is lower than at equilibrium since the temperature of the slower electrons is significantly lower than an estimated temperature based on the total absorbed x-ray energy. For harder x rays and larger focal diameters, in which case the system is not that strongly ionized, the difference in  $Z$  can be up to  $\Delta Z = 3$ . (ii) Since the electron distribution can be highly non-Maxwellian, an equilibrium electron temperature often cannot be defined, and the applicability of standard equilibrium models to describe the effects of the plasma environment on the atomic states, such as given by Stewart and Pyatt [11] and Eckart and Kroll [12], could be questionable. This is particularly an issue early on in the pulse. (iii) To study equilibrium plasmas using XFEL, longer pulses or, better, pump-probe setups with sufficient delays of up to hundreds of fs are required. (vi) Before the slow and fast electrons peaks equilibrate, the fast electrons also equilibrate among themselves and generate some electrons with kinetic energies that greatly exceed the photon energy. This needs to be taken into account when interpreting emission spectra of XFEL-irradiated materials [1].

### ACKNOWLEDGMENTS

This work was performed under the auspices of the US Department of Energy by Lawrence Livermore National Laboratory under Contract No. DE-AC52-07NA27344. The author would like to acknowledge useful discussions with J. Weisheit, D. Richards, and J. Glosli. Some of the simulations were performed on LLNL's Sequoia BlueGene/Q system.

- 
- [1] S. Vinko *et al.*, *Nature* **482**, 59 (2012).
  - [2] R. Fäustlin *et al.*, *Phys. Rev. Lett.* **104**, 125002 (2010).
  - [3] S. P. Hau-Riege *et al.*, *Phys. Rev. Lett.* **108**, 217402 (2012).
  - [4] T. Gorkhover *et al.*, *Phys. Rev. Lett.* **108**, 245005 (2012).
  - [5] S. Schorb *et al.*, *Phys. Rev. Lett.* **108**, 233401 (2012).
  - [6] H. Thomas *et al.*, *Phys. Rev. Lett.* **108**, 133401 (2012).
  - [7] S. Jamison, *Nat. Photon.* **4**, 589 (2010).
  - [8] N. Medvedev, U. Zastra, E. Forster, D. O. Gericke, and B. Rethfeld, *Phys. Rev. Lett.* **107**, 165003 (2011).
  - [9] D. A. Chapman and D. O. Gericke, *Phys. Rev. Lett.* **107**, 165004 (2011).
  - [10] W. Lotz, *Astrophys. J. Suppl.* **14**, 207 (1967).
  - [11] J. C. Stewart and K. D. Pyatt, Jr., *Astrophys. J.* **144**, 1203 (1966).
  - [12] G. Ecker and W. Kroll, *Phys. Fluids* **6**, 62 (1963).
  - [13] F. H. Streitz, J. N. Glosli, and M. V. Patel, *Phys. Rev. Lett.* **96**, 225701 (2006).
  - [14] L. Redecke *et al.*, *Science* **339**, 227 (2013).
  - [15] S. P. Hau-Riege, *Phys. Rev. Lett.* **108**, 238101 (2012).
  - [16] T. Dunn and A. A. Broyles, *Phys. Rev.* **157**, 156 (1967).
  - [17] J. N. Glosli, F. R. Graziani, R. M. More, M. S. Murillo, F. H. Streitz, M. P. Surh, L. X. Benedict, S. Hau-Riege, A. B. Langdon, and R. A. London, *Phys. Rev. E* **78**, 025401 (2008).
  - [18] S. P. Hau-Riege *et al.*, *New J. Phys.* **15**, 015011 (2013).